Electronic Supplementary Information for

Near-infrared photothermal conversion property of carbazole-based cocrystals with different degree of charge transfer

Pan Shi[a], Xiao-Xu Liu[a], Xia-Lin Dai[a], Tong-Bu Lu[b], Jia-Mei Chen[a]*

[a] *Tianjin Key Laboratory of Drug Targeting and Bioimaging, School of Chemistry and Chemical Engineering, Tianjin University of Technology, Tianjin 300384,*

[b] *Institute for New Energy Materials and Low Carbon Technologies, School of Materials Science and Engineering, Tianjin University of Technology, Tianjin 300384, China*

**Corresponding author: Jia-Mei Chen, E-mail address: chenjiamei@email.tjut.edu.cn*

Experimental

Materials. Carbazole (CZ), 3,6-Dichlorocarbazole (ClCZ), 3,6-Dibromocarbazole (BrCZ) and 7,7,8,8-tetracyanoquinodimethane (TCNQ) were purchased from Energy Chemical. All other reagents and chemicals were commercially available and used directly.

Synthesis of cocrystals. CZ/TCNQ (1:1), **ClCZ/TCNQ** (1:1) and **BrCZ/TCNQ** (1:1) were prepared by slurrying an equimolar mixture of TCNQ (40.8 mg, 0.2 mmol) and CZ (33.2mg, 0.2 mmol)/ClCZ (47.2 mg, 0.2 mmol)/BrCZ (65.0 mg, 0.2 mmol) in 1 mL of acetonitrile for 24 h at room temperature. The suspension was filtered and the obtained solid was dried under room temperature to obtain bulk black powdered samples. The yields were 67.4 mg and 91.1% for **CZ/TCNQ**, 86.2 mg and 97.9% for **ClCZ/TCNQ** and 97.2 mg and 91.9% for **BrCZ/TCNQ**. FT-IR (KBr, ν/cm^{-1}) for **CZ/TCNQ**: 3142 (C–H), 2218 (C≡N), 1544 (C=C); For **ClCZ/TCNQ**: 3144 (C–H), 2218 (C≡N), 1542 (C=C); For **BrCZ/TCNQ**: 3140 (C–H), 2218 (C≡N), 1542 (C=C). The above filtrates were left to slowly evaporate at room temperature and rod-shaped single crystals were harvested after about one week.

Characterization of cocrystals. Single crystal X-ray diffraction data were collected on an Agilent Technologies Gemini A Ultra system with graphite monochromated Cu Kα radiation (λ= 1.54178 Å) at 293.76 K. Cell refinement and data reduction were applied using the program CrysAlis^{PRO}. The structures were solved by the direct method using the Olex2 program and refined by the full-matrix least-squares method on F^2.[1] Powder X-ray diffraction (PXRD) patterns were obtained on a Rigaku SmartLab X-ray diffractometer equipped with a D/teX Ultra one-dimensional detector, using Cu Kα

radiation (λ = 1.541862 Å) generated at 40 kV and 150 mA. Each sample was placed on a silicon disk and measured over an angular range of 5-40 ° (2θ) with a step size of 0.0142 ° (2θ). The simulated PXRD patterns were obtained from the crystallographic information file (cif) of each cocrystal by a software of Mercury available free of charge via the internet at http://www.iucr.org. Differential scanning calorimetry (DSC) was recorded on a Netzsch DSC 200F3 instrument with nitrogen atmosphere. Each sample was placed on an aluminum sample pan and heated from 30 °C to the decomposition temperature of the sample at a heating rate of 10 °C/min. UV-Vis absorption spectra were collected on a Shimadzu UV-2600 spectrometer using an integrating sphere with $BaSO_4$ as a white standard. Photoluminescence emissions were measured on an Edinburgh FLS1000 spectrometer. Fourier transform infrared (FTIR) spectra were recorded using a Perkin-Elmer Frontier FT-IR Spectrometers with KBr pellets. Optical microscopy images were taken by a Nikon LV100NPOL. The temperature was measured with an IR thermal camera (Flir T540 Thermal Imaging Camera). The molecular orbital and energy levels of cocrystals and individual components were calculated by Gaussian 09 program at the B3LYP/6-31G (d) level of theory.

Calculations of photothermal conversion efficiency. The photothermal conversion efficiency of cocrystals was determined according to previous method.[2] Details are as follows:

Based on the total energy balance for this system,

$$\sum_i m_i C_{pi} \frac{dT}{dt} = Q_S - Q_{loss}$$

where m_i and $C_{p,i}$ are the mass and heat capacity of system components (cocrystal

samples and substrate), respectively. The mass of all the three cocrystals and substrate are 320.6 mg. The heat capacity of **CZ/TCNQ**, **ClCZ/TCNQ** and **BrCZ/TCNQ** was measured by differential scanning calorimetry (DSC) and sapphire method with values of 0.69, 0.78 and 0.76 J/g^{-1} K^{-1}, respectively. Q_s is the photothermal heat energy input by irradiating NIR laser to samples, and Q_{loss} is thermal energy lost to the surroundings. When the temperature reaches maximum, the system is in balance.

$$Q_S = Q_{loss} = hS\Delta T_{max}$$

where h is heat transfer coefficient, S is the surface area of the container, ΔT_{max} is the maximum temperature change. The photothermal conversion efficiency η is calculated from the following equation,

$$\eta = \frac{hS\Delta T_{max}}{I(1 - 10^{-A_{808}})}$$

where I is the laser power (0.48 W/cm^2) and A_{808} is the absorbance of the samples at the wavelength of 808 nm. In order to get the hS, a dimensionless driving force temperature, θ is introduced as follows,

$$\theta = \frac{T - T_{surr}}{T_{max} - T_{surr}}$$

where T is the temperature of cocrystal, $T_{\max}$ is the maximum system temperature, and T_{surr} is the initial temperature (22.2 °C). And a sample system time constant τ_s

$$\tau_s = \frac{\sum_i m_i C_{pi}}{hS}$$

Thus

$$\frac{\mathrm{d}\theta}{\mathrm{d}t} = \frac{Q_s}{\tau_s hS\Delta T_{max}} - \frac{\theta}{\tau_s}$$

When the laser is off, $Q_S = 0$, therefore

$$\frac{\mathrm{d}\theta}{\mathrm{d}t} = -\frac{\theta}{\tau_s}$$

and

$$t = -\tau_s \ln \theta$$

So hS could be calculated from the slope of cooling time vs $ln\theta$.

Table S1. Crystallographic data and refinement parameters of the cocrystals.

cocrystal	**CZ/TCNQ**[3]	**ClCZ/TCNQ**	**BrCZ/TCNQ**
chemical formula	$C_{24}H_{13}N_5$	$C_{24}H_{11}Cl_2N_5$	$C_{24}H_{11}Br_2N_5$
formula wt	371.40	440.28	529.20
temperature (K)	283-303	292.1(8)	293.7(10)
crystal size (mm^3)	/	0.1×0.05×0.08	0.10×0.05×0.06
crystal system	monoclinic	monoclinic	monoclinic
space group	*C 2/m*	*I 2/a*	*I* 2/*a*
a (Å)	11.249(4)	12.1500(2)	12.3323(4)
b (Å)	12.973(4)	13.1041(2)	13.1469(3)
c (Å)	6.674(1)	13.7735(2)	13.9845(5)
α (deg)	90	90	90
β (deg)	107.59(2)	112.503(2)	113.945(4)
γ (deg)	90	90	90
volume ($Å^3$)	928.42	2025.97(6)	2072.19(13)
Z	2	8	8
density (g/cm^3)	1.329	1.443	1.696
2*θ* range	/	4.844-79.194	4.826-79.102
F (000)	/	896	1040
index ranges	/	$-15 \le h \le 15$	$-15 \le h \le 15$
	/	$-16 \le k \le 16$	$-16 \le k \le 15$
	/	$-16 \le l \le 11$	$-16 \le l \le 17$
no. of reflns	/	2169	2197
no. of unique reflns	/	2070	2029
no. of params	/	141	159
R_{all}, R_{obs}[a]	/	0.0428, 0.0418	0.0366, 0.0352
w$R_{2,all}$, w$R_{2,obs}$[b]	/	0.1208, 0.1194	0.0963, 0.0951
Goodness-of-fit on F^2	/	1.065	1.135
CCDC No.	1121578	2154402	2154407

[a] $R_1 = \Sigma \, | \, |F_o| - |F_c| \, | / \Sigma \, |F_o|$. $wR_2 = [\Sigma[w(F_o^2 - F_c^2)^2]/\Sigma w(F_o^2)^2]^{1/2}$, $w = 1/[\sigma^2 (F_o)^2 + (aP)^2 + bP]$, where $P = [(F_o^2) + 2F_c^2]/3$

Table S2. Melting-point and melting enthalpy of the cocrystals.

cocrystal	melting-point (°C)	melting enthalpy (J/g)
CZ/TCNQ	304.2	147.3
ClCZ/TCNQ	274.7	142.0
BrCZ/TCNQ	273.3	136.1

Table S3. Calculations of photothermal conversion efficiency.

cocrystal	**CZ/TCNQ**	**ClCZ/TCNQ**	**BrCZ/TCNQ**
A_{808}	0.29	0.31	0.46
hS	2.72	2.79	2.91
T_{max}	69.1	65.5	56.7
ΔT	46.2	42.6	34.5
τ_s	90.8	88.6	84.9
η	53.7%	48.5%	32.0%

(a)

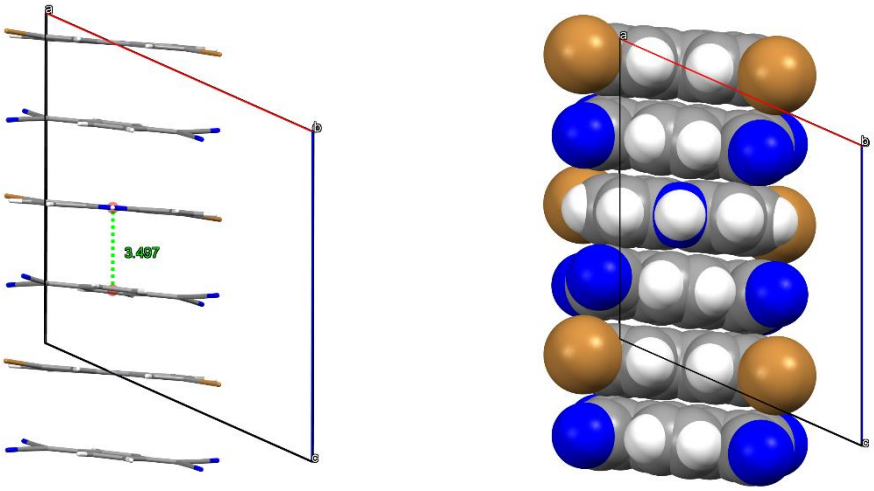

(b)

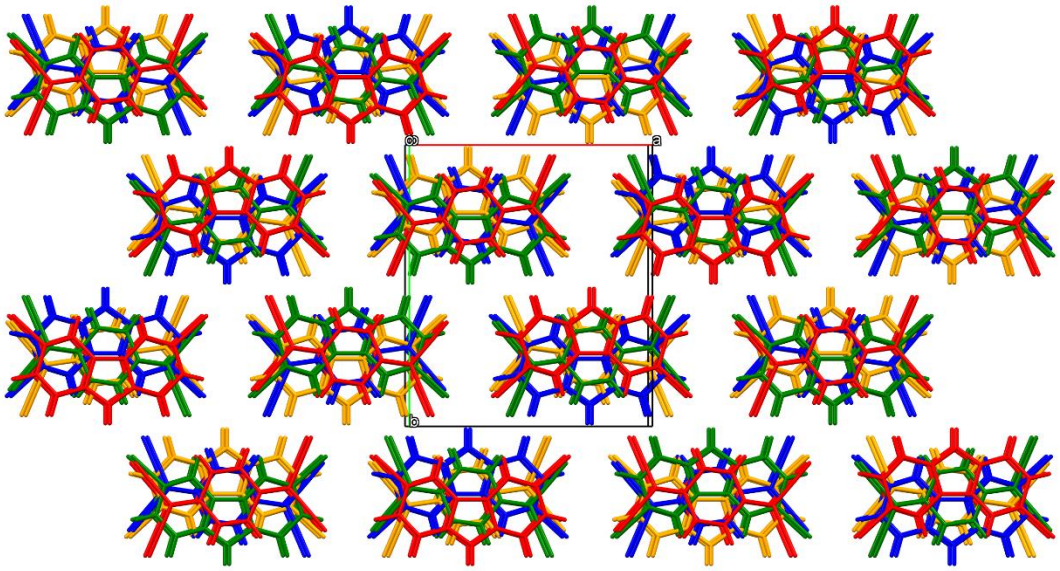

Fig. S1 (a) ···DADADA···column-like charge transfer structure, and (b) 3D packing pattern of **BrCZ/TCNQ**.

(a)

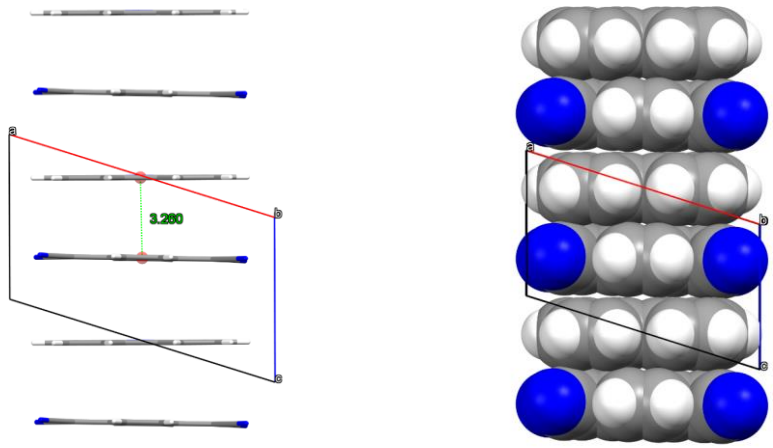

(b)

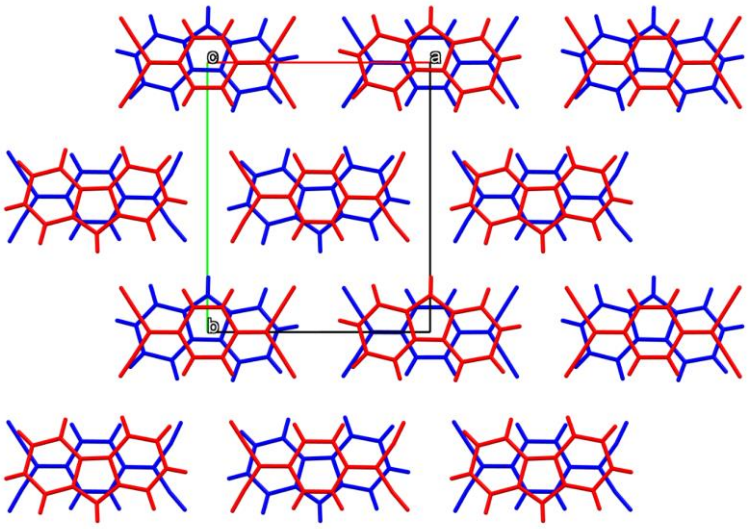

Fig. S2 (a) ···DADADA···column-like charge transfer structure, and (b) 3D packing pattern of **CZ/TCNQ**.

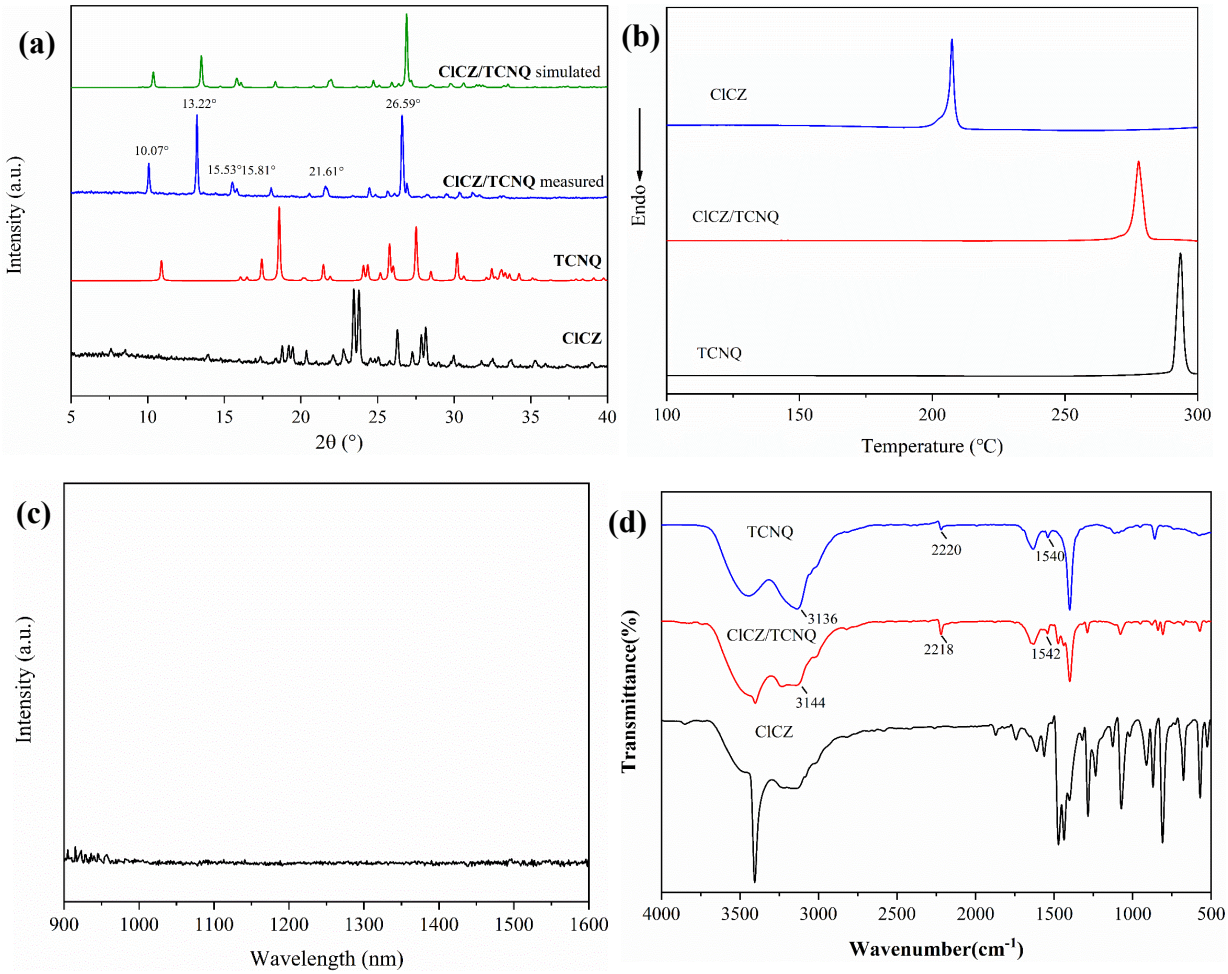

Fig. S3 (a) PXRD patterns, and (b) DSC curves of **ClCZ/TCNQ** and individual components. (c) NIR emission spectrum of **ClCZ/TCNQ**. (d) IR spectra of **ClCZ/TCNQ** and individual components.

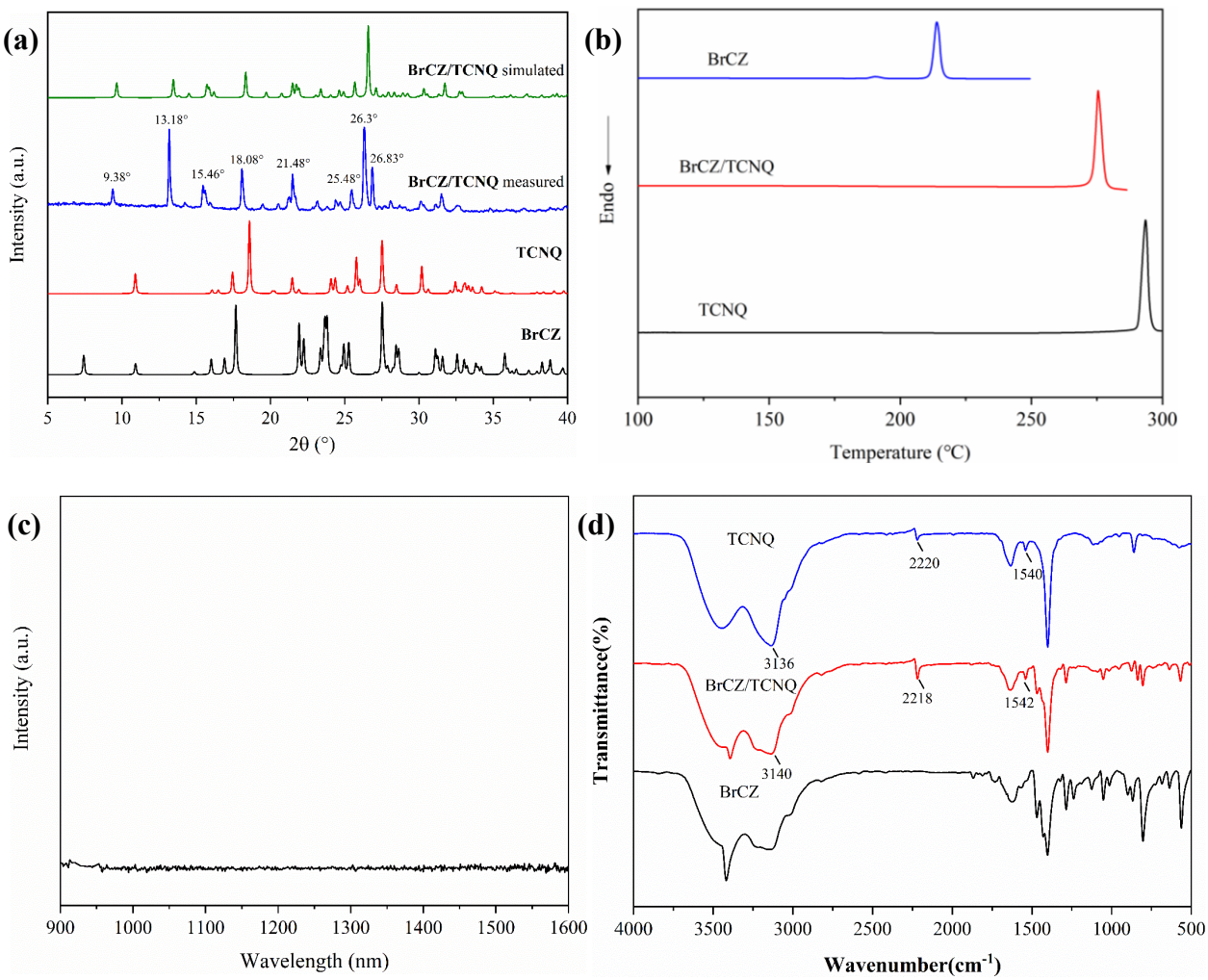

Fig. S4 (a) PXRD patterns, and (b) DSC curves of **BrCZ/TCNQ** and individual components. (c) NIR emission spectrum of **BrCZ/TCNQ**. (d) IR spectra of **BrCZ/TCNQ** and individual components.

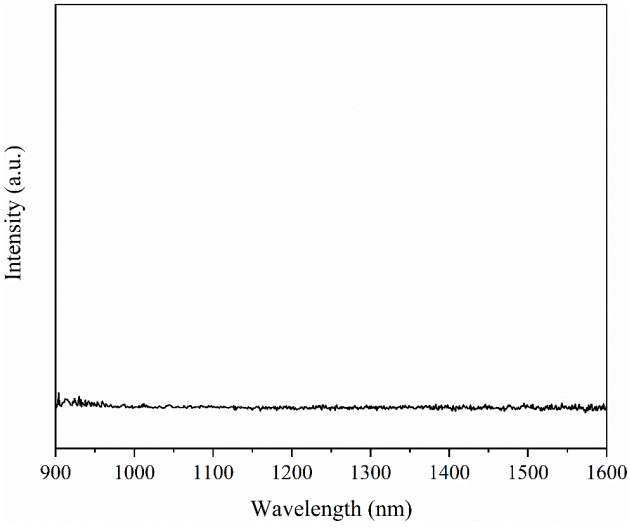

Fig. S5 NIR emission spectrum of **CZ/TCNQ**.

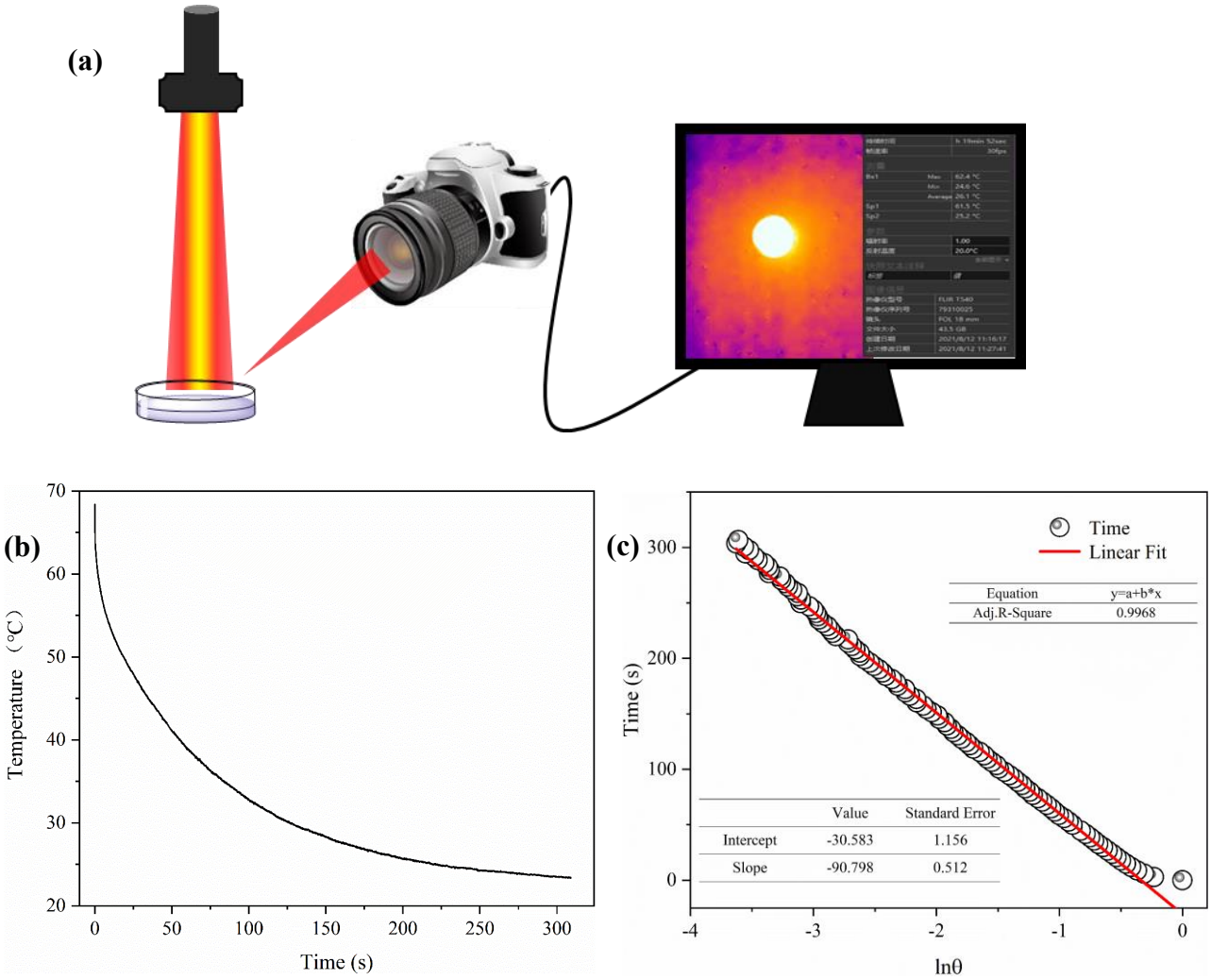

Fig. S6 (a) Diagram of the photothermal conversion measurement. (b) The cooling curve of **CZ/TCNQ** after 808 nm laser irradiation, and (c) the time-lnθ linear curve.

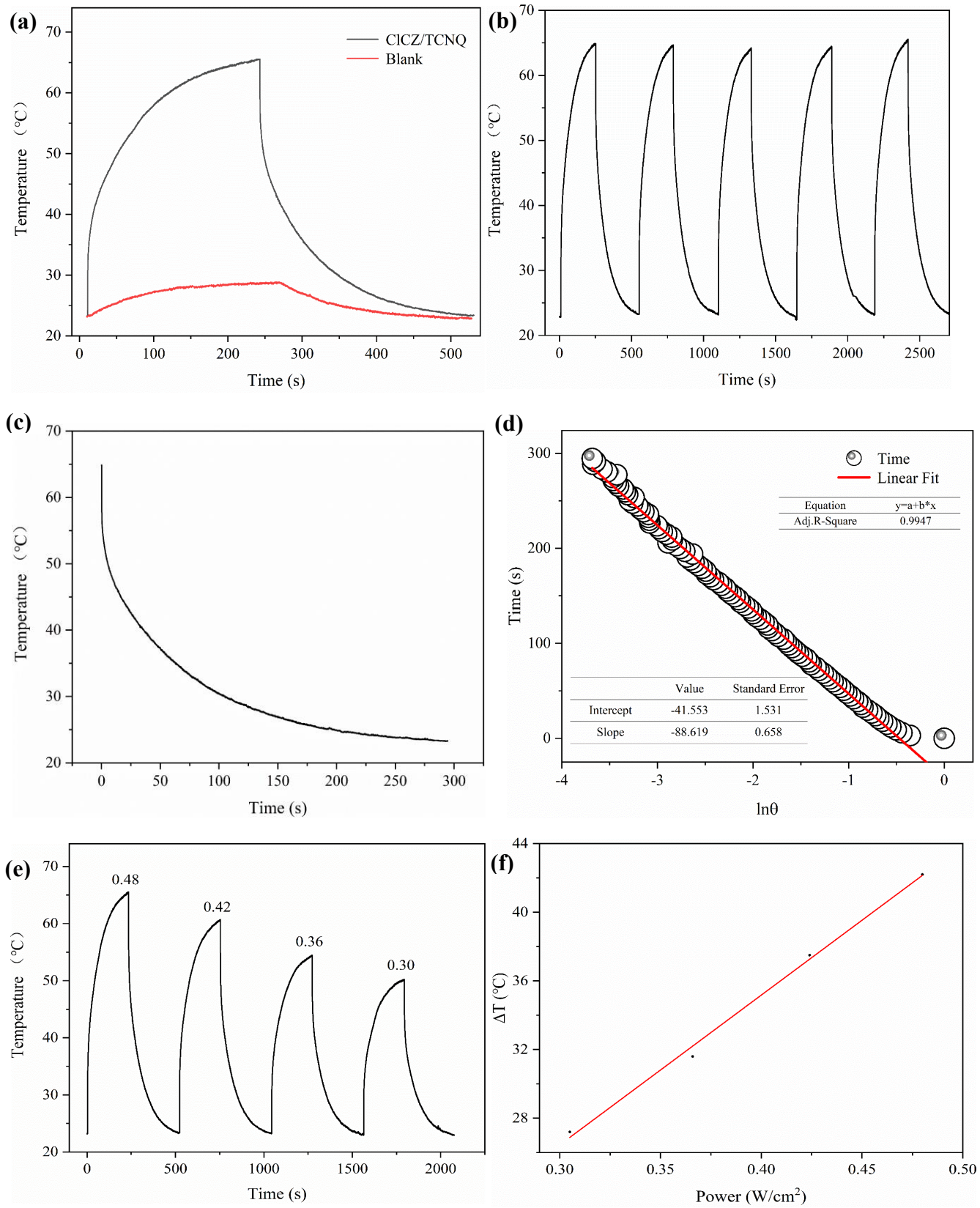

Fig. S7 (a) Temperature profile and (b) photothermal conversion cyclic test of **ClCZ/TCNQ** under 808 nm laser irradiation (0.48 W/cm^2). (c) The cooling curve of **ClCZ/TCNQ** after 808 nm laser irradiation, and (d) the time-lnθ linear curve. (e) Temperature profile of **ClCZ/TCNQ** at different powers (W/cm^2), and (f) the linear relationship between ΔT and 808 nm laser power.

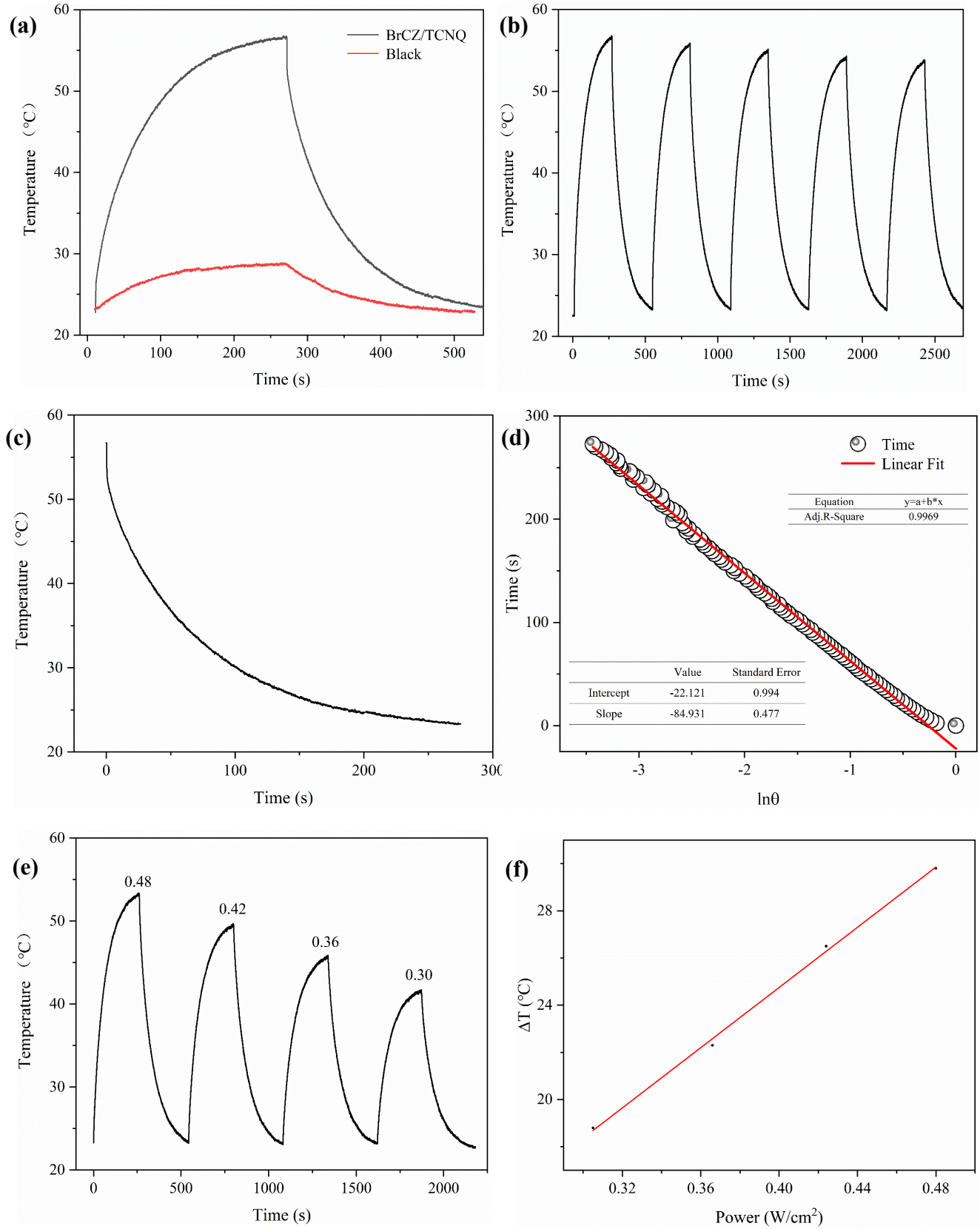

Fig. S8 (a) Temperature profile and (b) photothermal conversion cyclic test of **BrCZ/TCNQ** under 808 nm laser irradiation (0.48 W/cm^2). (c) The cooling curve of **BrCZ/TCNQ** after 808 nm laser irradiation, and (d) the time-lnθ linear curve. (e) Temperature profile of **BrCZ/TCNQ** at different powers (W/cm^2), and (f) the linear relationship between ΔT and 808 nm laser power.

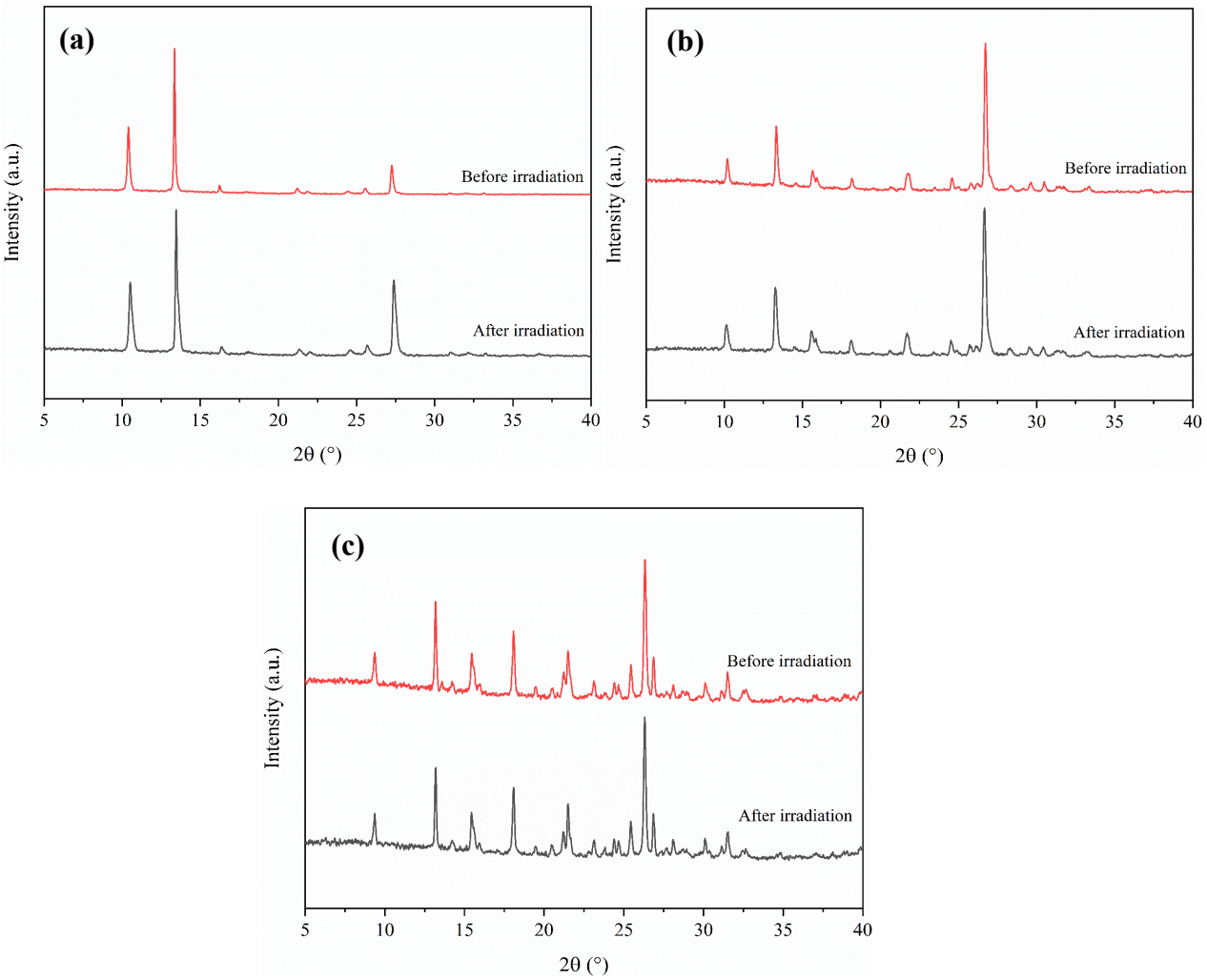

Fig. S9 PXRD patterns of **CZ/TCNQ**, **ClCZ/TCNQ** and **BrCZ/TCNQ** before and after 808 nm laser irradiation.

References

1 O. V. Dolomanov, L. J. Bourhis, R. J. Gildea, J. A. K. Howard, H. Puschmann, OLEX2: a complete structure solution, refinement and analysis program. *Journal of Applied Crystallography*, 2009, **42**, 339−341.

2 Y. Wang, W. G. Zhu, W. N. Du, X. F. Liu, X. T. Zhang, H. L. Dong and W. P. Hu, *Angewandte Chemie, International Edition*, 2018, **57**, 3963−3967.

3 V. V. Mitkevich and L. F. Sukhodub, *Kristallografiya*, 1986, **31**, 815−817.